About the dynamic characterization of micro-bolometric infrared cameras

Diego Scaccabarozzi*, Bortolino Saggin

Politecnico di Milano, Dipartimento di Meccanica Polo Territoriale di Lecco, Via G. Previati 1c, 23900 Lecco, Italy

1. Introduction

Uncooled microbolometers have been developed since the 1980s aiming at producing low cost IR imaging systems mostly for military applications [1,2]. Thanks to their small size, high reliability, low power consumption, possibility to be used at ambient temperature and most of all the dramatic cost reduction, in the last years they have experienced wide spreading in many industrial and civil applications, such as search and rescue [3], environmental protection, driver's vision assistance [4], energy conservation, fire detection [5] and medical imaging [6,7].

A resistive microbolometer absorbs infrared radiation from the observed scene and changes its electrical resistance according to its temperature increase. Change of the resistance is usually sensed by biasing the sensor through a constant current or voltage. The sensing element is by design thermally insulated from the supporting structure whose thermal conductivity determines the detector sensitivity and its dynamic performance [8]. Improving the thermal insulation increases the microbolometer sensitivity at the detriment of the dynamic response therefore, a trade-off between these opposite requirements is performed. At present, VOx microbolometer arrays are the state of the art in infrared uncooled technology thanks to their high sensitivity, even though currently and likely in the near future, a-Si and new silicon based materials are the most common thanks to their lower cost and easier manufacturability [9]. The dynamic performances of microbolometers have been already addressed in literature, e.g. in Refs. [2,4,10–15] and [16–19] or [20], highlighting time constant ranging between 10 and 30 ms, mainly derived from theoretical computation and seldom supported by any testing. To achieve signals compatible with traditional analogic video standards sampling rate of 30 Hz or 60 Hz are quite common, despite only the lowest time constants mentioned above allow exploiting the sampling rate without major dynamic errors. In conclusion, sampling rate is not an indicator of the actual dynamic performances for this kind of instruments and the time constant is not commonly indicated among the instrument characteristics. Thus, an experimental characterization is generally required.

This work describes two methods for the assessment of the dynamic characteristics of a microbolometer, which are derived from the commonly adopted methods for the determination of the time constant in first order systems. Both methods have been applied to a TH7102WX NEC infrared camera equipped with a 320×240 pixels microbolometer. The paper is organized as follows: Section 2 introduces and describes the methods used for the dynamic characterization and provides the related uncertainty budgets. Section 3 shows test results that are discussed in Section 4. Conclusions are eventually drawn in Section 5.

* Corresponding author.
E-mail address: diego.scaccabarozzi@polimi.it (D. Scaccabarozzi).

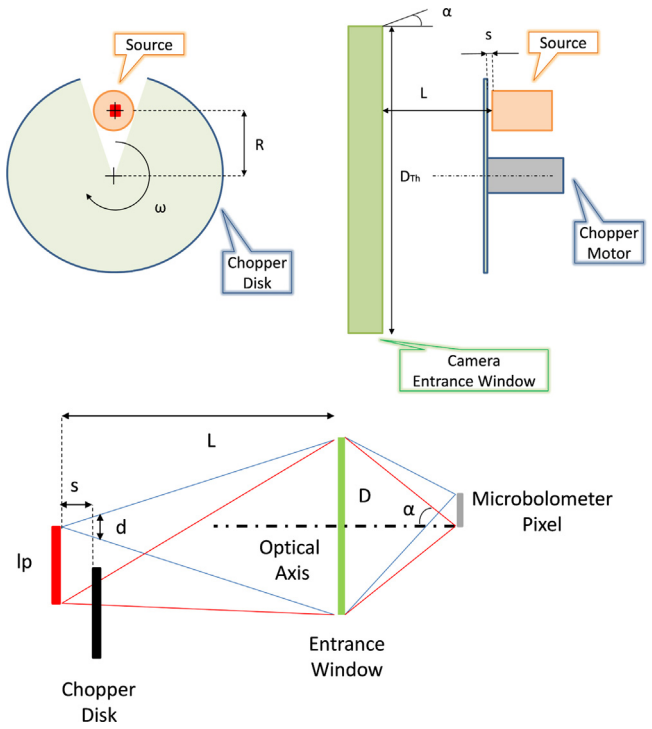

Fig. 1. Setup for the microbolometer dynamic calibration. (Bottom) Schematic to evaluate the time of the ramp signal.

2. Material and methods

2.1. Background

Step input response is a simple technique commonly exploited to extract the dynamic characteristics of mechanical, electrical and thermal systems. For thermal imaging systems, as the microbolometer tested in our study, this input can be obtained by moving a hot source in the FOV (Field of View) of the system looking to a colder background. Alternatively, to avoid moving the source, a shutter mechanism can be employed: the source is positioned behind the shutter that cyclically opens and closes a window so that in the camera FOV the hot source alternates with the cold shutter blade. A scheme of the setup is shown in Fig. 1. A chopper generates a square wave like signal whose frequency is proportional to the disc angular speed. This periodic input is commonly used in infrared detectors testing to differentiate between the dark current signal, due to the detector noise, and the true signal [21]. Anyway, if the chopper opening and the sensor output are measured, the frequency response function (FRF) $H(i\omega_p)$ of the microbolometer can be computed through their Fourier Transforms:

$$H(i\omega) = \frac{O(i\omega_p)}{I(i\omega_p)} \tag{1}$$

where $O(i\omega_p)$ and $I(i\omega_p)$ are respectively the FFTs (Fast Fourier Transforms) of the sensor and the chopper signals and ω_p is the angular frequency.

If the microbolometer can be modelled as a first order system, its FRF can be-written as:

$$H(i\omega_p) = \frac{O(i\omega_p)}{I(i\omega_p)} = \frac{k}{1 + i\omega_p\tau} \tag{2}$$

where k is the detector sensitivity and τ is the microbolometer time constant. If ω_p varies in the range of interest, τ and k can be retrieved with Eq. (2) from a parametric fit of experimental data.

The measured signal can be analyzed in the time domain as well. In case of an ideal step input measured time response is expected to be an exponential as in the following:

$$T(t) = T_f + (T_i - T_f)e^{\frac{t}{\tau}} \tag{3}$$

where T_i and T_f are the initial and final temperatures. Rewriting Eq. (2) in logarithm scale, one can write:

$$Z(t) = \ln\left(\frac{T(t) - T_f}{T_i - T_f}\right) = \frac{-t}{\tau} \tag{4}$$

where the slope of $Z(t)$ provides the reciprocal of τ. The slope can be obtained from the best fit of $Z(t)$ [22].

Summarizing, both approaches can be applied to derive the microbolometer time constant from the measured response to a step temperature input.

2.2. Setup design

The setup exploited a "Scitec 300D" chopper with the two apertures rotating disc that has an outer diameter of 102 mm. One of the two sectors was eventually shut to provide a single aperture of 90° angular span. The distance of the source from the chopper rotation axis was 40 mm. The source was an aluminium cylinder of 20 mm diameter, heated at different temperatures through an electrical film resistor. The source temperature was measured by a K type thermocouple incorporated in the cylinder whose surface was coated with the high emissivity paint Electrodag501®.

In order to achieve a step input close to the ideal one, the rise time (i.e. the time taken by the shutter border to sweep across the pixel area) should be negligible in comparison with the expected time constant. The chopper disc tangential speed depends on its angular speed ω_{ch} and on the distance R of the source from the chopper rotation axis:

$$v = \omega_{ch}R = 2\pi f_{ch}R \tag{5}$$

The pixel size l_p can be determined by the focal distance L and the instrument IFOV (Instantaneous Field of View) 2α:

$$l_p = \tan(\alpha)L \tag{6}$$

Moreover, an additional distance, identified in Fig. 1b as d, has to be covered to complete the microbolometer pixel release. This distance depends on the distance s between the source and the chopper disc as:

$$d = \frac{D}{L}s \tag{7}$$

where D is the entrance diameter of the infrared camera.

Combination of above defined contributions leads to the definition of the rise time as:

$$t_p = \frac{lp + d}{v} \tag{8}$$

In order to reduce as much as possible t_p the setup designer has three possibilities:

- reducing L to the minimum one allowed by the tested camera in order to decrease the pixel size l_p; and
- increasing the tangential speed v by enlarging the distance R or the chopper frequency; and
- reducing the distance s between the chopper disc and the source.

In order to avoid aliasing problem the maximum camera sampling frequency limits the chopper frequency; in our case, the maximum sampling rate is 30 Hz.

Anyway, if t_p is one order magnitude lower than the microbolometer time constant, the discrepancy between real and

Table 1
Summary of the setup geometry.

Parameter	Value
L (mm)	500
D (mm)	48
R (mm)	35
s (mm)	3
IFOV (mrad)	1.58

ideal step inputs becomes negligible. For the implemented setup t_p is expected between 0.5 and 5 ms, whereas the foreseen τ is in the range of (10–30) ms therefore, even in the best case of the largest time constant, the assumption of ideal step input is not acceptable. Thus, the ramp transient was accounted in the input signal. Geometry of the final setup, the optical configuration and geometry constraints for the dynamic characterization are summarized in Table 1.

2.3. Uncertainty budgets

2.3.1. Uncertainty budget FRF method

The uncertainty of the time constant measurement has been determined by numerical simulation, according to Ref. [23]. The simulation parameters are reported in the following:

- chopping frequency f_{ch} was varied between 1 and 6 Hz at fixed steps depending on the number of chopping frequencies;
- number N of the chopping frequencies for the FRF reconstruction was changed between 6 and 21;
- microbolometer time constant τ ranged from 5 to 50 ms;
- step input initial temperature T_i was set at 25 °C;
- final step input temperature T_f settled at 60, 80 and 100 °C.

The temperature uncertainty assigned to T_i and T_f in the numerical propagation was evaluated with a repeatability assessment performed on the infrared camera. Analysis of 300 frames of a blackbody allowed evaluating the pixel repeatability. Fig. 2 shows the measured temperature standard deviation in the acquired images. Standard deviation looks symmetrical w.r.t. the sensor middle along the image rows and increases up to 0.2 °C in the pixels near the image edges. Along the columns instead the behaviour seems to be uniform. The maximum temperature standard deviation of 0.2 °C was used for the whole sensor's area as a worst-case to derive the time constant uncertainty.

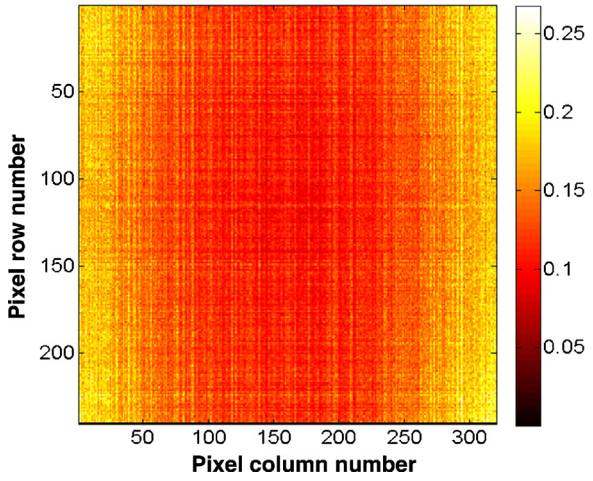

Fig. 2. Temperature standard deviation over the infrared image of a black body. Colour scale is °C unit.

Real step input was modelled with a temperature ramp whose rise time was calculated according to Eqs. (5)–(8). The overall simulation time was set to 10 s. Fig. 3 provides flowchart of the simulation: microbolometer time response and the ramp input are resampled at 30 Hz and digitally filtered (Chebyshev type, 8th order, cut-off frequency at 0.9 the Nyquist frequency) in order to avoid aliasing in computed spectra. Fig. 3 shows simulated responses at constant chopping frequency with different time constants and noise addition.

Computed relative uncertainty varies from a maximum of 12% at 5 ms to 4% at 50 ms. Moreover, low uncertainty (less than 5%) is obtained for τ in 10–30 ms range. No significant differences were highlighted varying N for time constants between 10 and 50 ms. Thus, N was finally set to 11, value identified as the best tradeoff between experimental effort and expected uncertainty.

Moreover, general conclusions can be drawn by the performed analyses. The uncertainty generally increases with time constants below 10 ms because of the limited sampling frequency of the infrared camera (i.e. 30 Hz) that does not permit measuring the sensor dynamic for the lowest time constants. Finally, accuracy of the proposed procedure worsens with the increasing of τ. This effect can be reduced by decreasing the chopper frequency range so that even in case of large time constant, time response is adequate to perform the FRF computation.

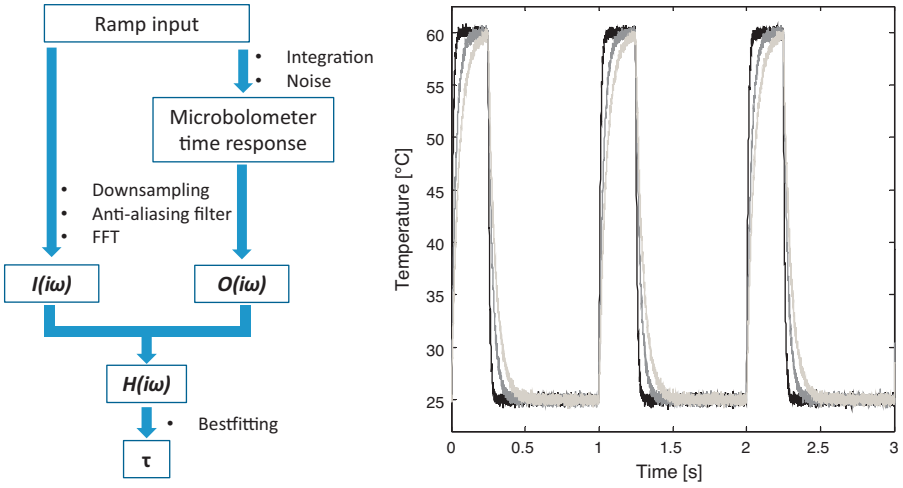

Fig. 3. (Left) Simulation flowchart. (Right) Simulated temperatures with different time constants and fixed chopping frequency, i.e. 10 ms (black), 30 ms (dark grey) and 50 ms (light grey).

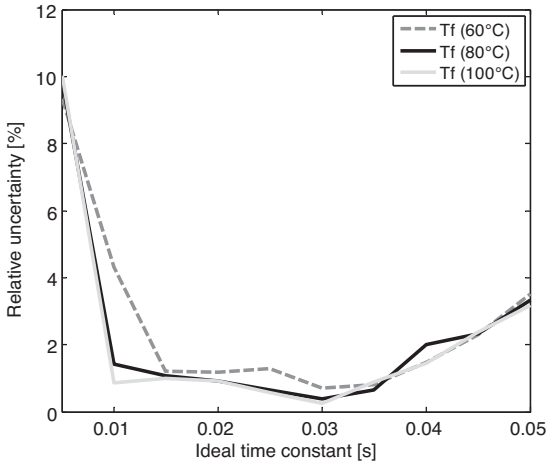

Fig. 4. Relative uncertainty for different step inputs and with N set to 11.

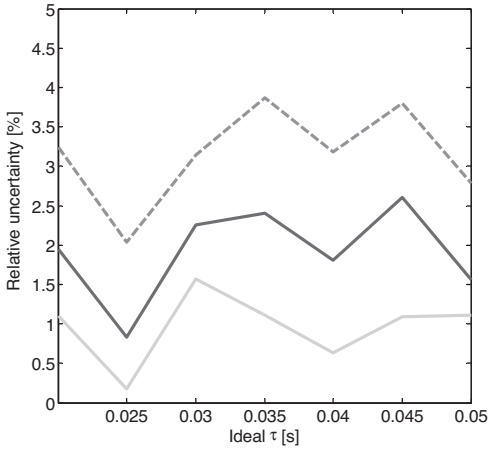

Fig. 5. Uncertainty budget for the time based method with different final temperatures, i.e., 60 °C (dashed curve), 80 °C (black) and 100 °C (light grey).

Comparison of the obtained relative uncertainty in the case of different temperature steps and with fixed N (set to 11) is shown in Fig. 4. No noticeable differences can be evidenced, highlighting that the contribution of the detector noise is negligible.

2.3.2. Uncertainty budget for the time based method

Uncertainty was evaluated with the following parameters:

- chopping frequency f_{ch} at 1 Hz;
- microbolometer time constant τ ranging from 20 to 50 ms.

The initial and final temperatures were set at the same values used for the FRF method.

Detector noise, derived by the preliminary testing, was added to the simulated signal (as shown in Fig. 3). f_{ch} has been chosen as the lowest stable chopper frequency in order to maximize the range on which performing the best fit. Time constants lower than 20 ms were not investigated due to the constraint imposed by the camera sampling frequency. This figure is more critical than in the FRF method since reducing further the time constant reduces the points that can be used to perform the best fit of $Z(t)$. These points are in fact those differing from the steady state more than the measurement noise.

Relative uncertainties with different step amplitudes are almost constant and restrained to a maximum of 4%, as shown in Fig. 5. Moreover, it can be shown that by increasing the amplitude of the step input, the relative uncertainty reduces to about 1% thanks to the reduction of the effect of the microbolometer noise with respect to the dynamic part of the signal on the measured temperature.

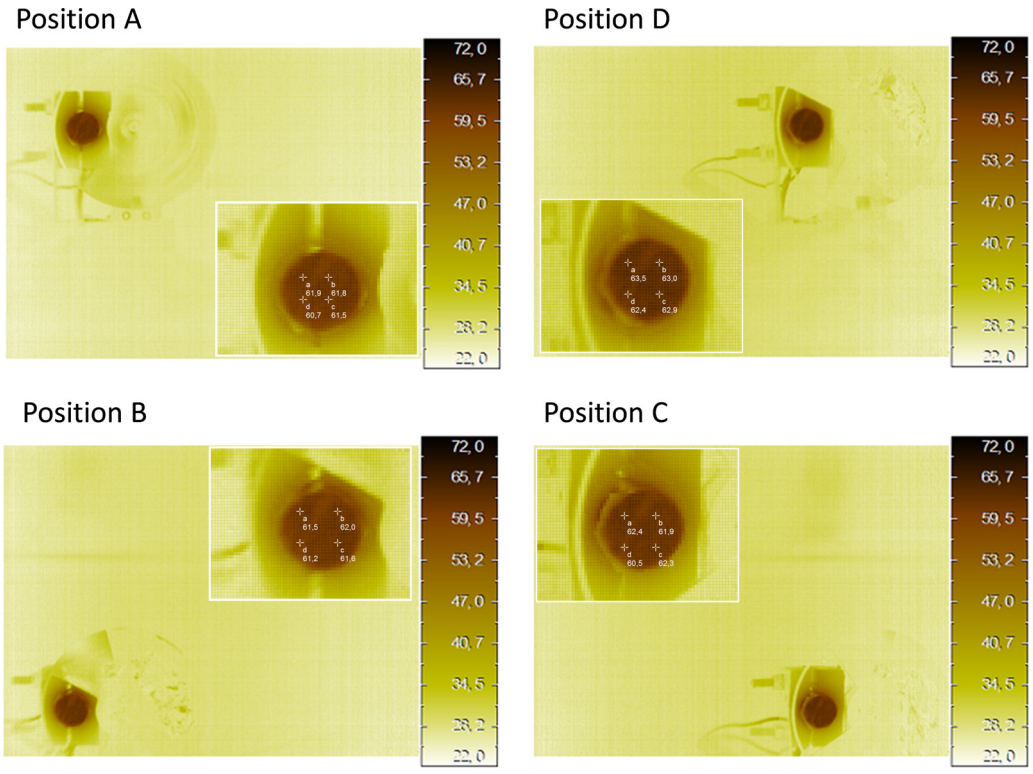

Fig. 6. Selected areas for the microbolometer dynamic testing.

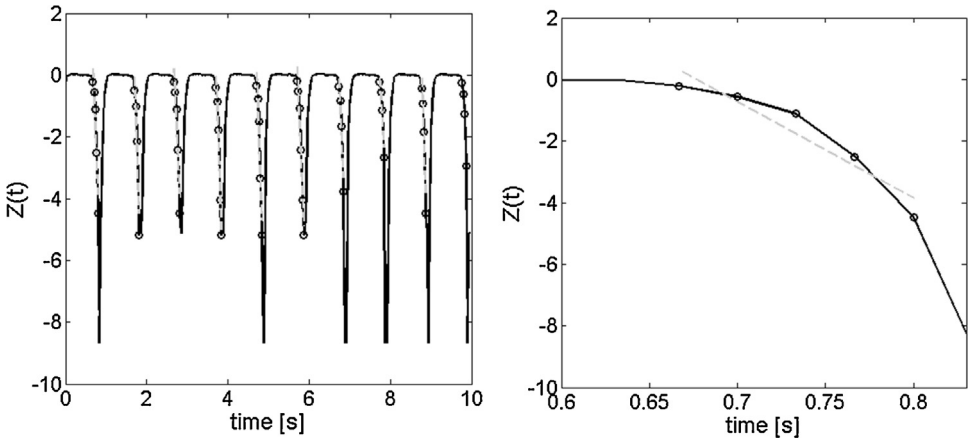

Fig. 7. Left: Best fit of the experimental data for 1 Hz chopping frequency (position B) with the time based method. Right: Zoom of the fit around 0.7 s.

Table 2
Time constants extracted with the time based method.

Position	Average (ms)	Repeatability %
A	27.3	8.4
B	28.3	8.7
C	26.1	8.1
D	29.1	4.9

Table 3
Time constants extracted with the FRF method.

Position	Average (ms)	Repeatability %
A	52.0	2.1
B	52.4	2.3
C	54.4	3.6
D	52.8	2.4

3. Experimental activity

Microbolometer performances have been evaluated in four different positions as shown in Fig. 6 to assess the uniformity of the microbolometer matrix. In every position, the source temperature was stabilized at about 60 °C and measured by means of the internal thermocouple. For each position, time responses of 10 pixels around the centre of the source were extracted and analyzed. Average time constants, determined with the proposed methods, are shown in Tables 2 and 3. Fig. 7 shows the best fit of $Z(t)$ for a time history acquired with chopper frequency of 1 Hz and the infrared camera as in position B. Fig. 7 provides also a blow-up of the best fit around 0.7 s where, one can notice the strong deviation of the data from the first order model. Computed FRF of the same pixels is provided in Fig. 8.

Fig. 9 shows the measured temperature with 1 Hz chopping frequency and the camera in position B. Fit of the microbolometer time response with the time constants derived from the methods is shown in Fig. 9 as well. Fig. 10 shows data fitting increasing the model order. Computed time constants are provided in Table 4, with related fitting errors.

Table 4
Time constants extracted with the time and frequency based methods changing the model's order.

Order	Time constants (ms)	Error (°C)
1st (Time)	28	19.4
1st (FRF)	53	9.3
2nd (FRF)	33.30, 33.28	3.8

4. Discussion

Time domain method provided an average time constant of about 28 ms (Table 2), with measurement repeatability of about 8%. Completely different result is achieved with the fit in the frequency domain (see Fig. 8), which provided an average time constant almost twice (Table 3), i.e. 53 ms average. The latter method showed a repeatability of 2.5%. It has to be noticed that the matching of FRF is quite rapidly worsening if one includes the frequency range above 4 Hz. Thus, to achieve a better representation for the range where attenuation is still acceptable, the time constants have been extracted limiting the frequency range to 4 Hz.

Discrepancy between the methods is easily understood looking to the $Z(t)$ zoom shown in Fig. 7. The initial point where $Z(t)$ starts decreasing is neglected in the fit because the temperature input measured by the microbolometer is a real step, therefore, this part is affected by the rise time t_p. In our case, combination of the setup geometry and chopping frequency led to maximum rise time of about 6 ms that is anyway, only about 20% of the sampling time. Thus, only the first point of $Z(t)$ was neglected.

The trend of the $Z(t)$ is evidently not a line as would be expected by Eq. (4), even excluding the initial point affected by the non-ideal step input.

In Fig. 9 (right) responses of a system having the time constants derived from the methods are compared: changing the time constant from 28 to 53 ms (plots with black and grey colours), reduces the fit error of about 50%. Anyway, the achieved result still leads to large residual errors.

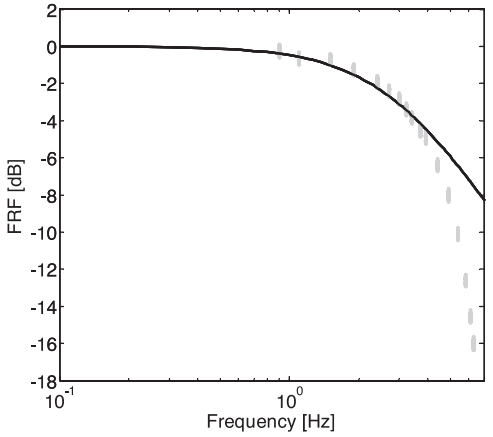

Fig. 8. Best fit of the experimental data (light grey dots) acquired in position B with the frequency based method.

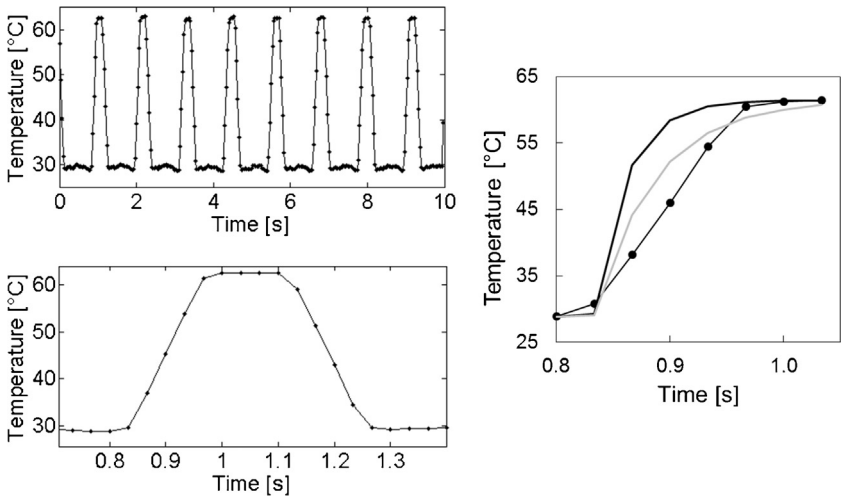

Fig. 9. Left: Full temperature time history (above) with lowest chopping frequency and zoom around 0.8 s (bottom). Right: Fitting curves of the experimental data with the measured time constants. Black and grey curves represent, respectively, time based and frequency-based methods.

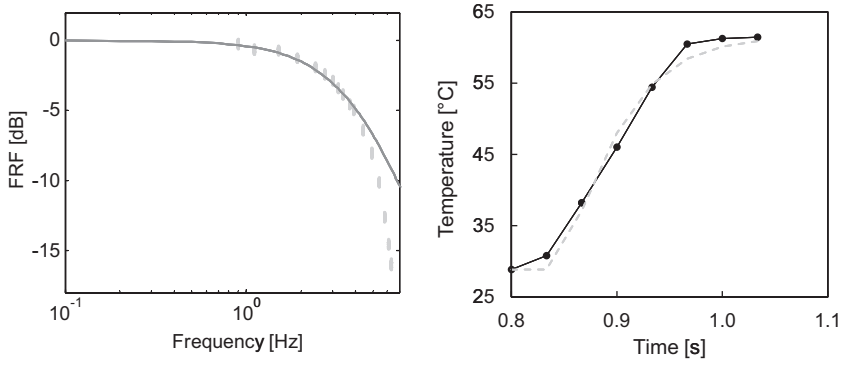

Fig. 10. (Left) 2nd order FRF. (Right) Best fitting curve of the micro-bolometer's time response with second order model.

This suggests increasing the order of the differential equations that models the thermal behaviour of the microbolometer. Second order systems have proved effective in modelling thermometers [24], with insulating structures i.e. systems quite similar to the microbolometer therefore, the identification of the parameters for such a kind of model has been performed as well.

A better matching is achieved with the 2nd order model, as shown in Fig. 10 where FRF and time response are provided. Enhanced matching is proved also by the residual error reported in Table 4, which strongly reduces with the second order model. Two almost identical thermal constants have been found from the FRF best fit. As done for the 1st order model, curve fitting was performed on the measured data up to 4 Hz.

From all that, it can be concluded that in the case study, the 1st order model does not allow to describe the microbolometer' behaviour even accepting modelling errors in the range of about 10 °C for a step input of about 40 °C; this is about one order of magnitude larger than the static accuracy. The adoption of a second order model improves the modelling accuracy with a reduction of the error in the step input response prediction by about a factor 3 but deviations larger than the static accuracy are still found.

The rather unsatisfying conclusion is that neither the first nor the second order model provide an effective modelling of this kind of detector. Thus, the usage of a time constant (or two time constants) appears unjustified and can be strongly misleading. If one is interested in defining the microbolometer' dynamic performance, the only effective ways seems to be the usage of the FRF or of the bandwidth definition.

A typical pass band criterion is identifying the frequency at which the output is attenuated by 3 dB. With this criterion in the case study, the microbolometer pass band upper limit is around 3 Hz (see Fig. 8), which is ten times lower than the sampling frequency.

5. Conclusions

Two methods for determining the time constant of infrared sensors have been applied to a commercial infrared camera equipped with an uncooled microbolometer. One method is based on the determination of the detector's frequency response function whereas the second approach uses the measured time history with a real step input.

Uncertainty of the exploited methods has been preliminarily assessed by means of numerical simulations aiming to design the experimental setup with a trade-off between measurement efforts and accuracy. Maximum uncertainty of the FRF based method is lower than 5% in case of detector time constants down to 10 ms whereas reduces to 2% for time constants larger than 30 ms. Uncertainty of the time-based procedure is always below 4% for time constants in the range between 20 and 50 ms.

Both methods were adopted to characterize a commercial infrared camera. The FRF method evidenced good repeatability, about 2%, fully compatible with the numerical simulations. Time based method conversely exhibited a repeatability in the order of 8%, about twice the expected for time constant varying between 30

and 50 ms. Moreover, the time constants measured by the methods were not compatible with differences of more than 30%. Results analysis evidenced that a first order model cannot represent the system behaviour even allowing for errors significantly larger than the static accuracy. The implementation of a second order model, though allowing a significant reduction in the modelling errors, still leaded to unsatisfying results if one considers the full frequency band up to 15 Hz allowed by the sampling frequency. The unexpected conclusion is that, at least for the characterized instrument, the only effective dynamic characterization is through the FRF, which, by the way, shows that even accepting errors up to 3 dB in the modulus, the pass band is limited to 3 Hz, i.e. one fifth of the maximum frequency allowed by the device' sampling rate.

References

[1] A. Rogalski, Infrared detectors: status and trends, Prog. Quantum Electron. 27 (2003) 59–210.
[2] J.L. Tissot, IR detection with uncooled sensors, Infrared Phys. Technol. 46 (2004) 147–153.
[3] B.D. Figler, Microbolometer uncooled thermal imaging sensors for law enforcement applications. Enabling Technologies for Law Enforcement, in: International Society for Optics and Photonics, 2001, pp. 195–205.
[4] T. Breen, N. Butler, M. Kohin, C.A. Marshall, R. Murphy, T. Parker, et al., Summary of applications of uncooled microbolometer sensors, in: IEEE Aerospace Applications Conference Proceedings, 3, 1999, pp. 361–374.
[5] G.L. Francisco, Amorphous silicon bolometer for fire/rescue. Aerospace/Defense Sensing, Simulation, and Controls, in: International Society for Optics and Photonics, 2001, pp. 138–148.
[6] N.A. Diakides, J.D. Bronzino, Medical Infrared Imaging, CRC Press, 2007.
[7] M. Tarabini, B. Saggin, D. Scaccabarozzi, G. Lanfranchi, Estimation of the orthosis-limb contact pressure through thermal imaging, in: Instrumentation and Measurement Technology Conference (I2MTC) 2012 IEEE International, IEEE, 2012, pp. 2733–2737.
[8] P.W. Kruse, Uncooled Thermal Imaging: Arrays, Systems, and Applications, SPIE Press, Bellingham, WA, 2001.
[9] A. Rogalski, Recent progress in infrared detector technologies, Infrared Phys. Technol. 54 (2011) 136–154.
[10] W.A. Lentz, Characterization of Noise in Uncooled IR Bolometer Arrays, Massachusetts Institute of Technology, 1998.
[11] W.A. Radford, D.F. Murphy, J.A. Finch, K. Hay, A. Kennedy, M. Ray, et al., Sensitivity improvements in uncooled microbolometer FPAs, in: AeroSense'99, International Society for Optics and Photonics, 1999, pp. 119–130.
[12] C. Chen, X. Yi, X. Zhao, B. Xiong, Characterizations of VO_2-based uncooled microbolometer linear array, Sens. Actuators A: Phys. 90 (2001) 212–214.
[13] L. Becker, Influence of IR sensor technology on the military and civil defense, in: Integrated Optoelectronic Devices 2006, International Society for Optics and Photonics, 2006, pp. 61270S-S-15.
[14] J. LaVeigne, G. Franks, K. Sparkman, M. Prewarski, B. Nehring, S. McHugh, LWIR NUC using an uncooled microbolometer camera, SPIE Defense, Security, and Sensing, in: International Society for Optics and Photonics, 2010, pp. 766306–766309.
[15] A. Rogalski, Progress in focal plane array technologies, Prog. Quantum Electron. 36 (2012) 342–473.
[16] R. Wood, C. Han, P. Kruse, Integrated uncooled infrared detector imaging arrays, in: Solid-State Sensor and Actuator Workshop, 1992 5th Technical Digest, IEEE, 1992, pp. 132–135.
[17] R. Wood, High-performance infrared thermal imaging with monolithic silicon focal planes operating at room temperature, in: Electron Devices Meeting, 1993 IEDM'93 Technical Digest, International, IEEE, 1993, pp. 175–177.
[18] U. Mizrahi, A. Fraenkel, L. Bykov, A. Giladi, A. Adin, E. Ilan, et al., Uncooled detector development program at SCD, Defense and Security, in: International Society for Optics and Photonics, 2005, pp. 551–558.
[19] C. Minassian, J.L. Tissot, M. Vilain, O. Legras, S. Tinnes, B. Fieque, et al., Uncooled amorphous silicon TEC-less 1/4 VGA IRFPA with 25 μm pixel-pitch for high volume applications, in: SPIE Defense and Security Symposium, International Society for Optics and Photonics, 2008, pp. 69401Z-Z-8.
[20] E. Zappa, A. Cigada, F. Romanò, R. Sala, On the Static and Dynamic Characterisation of Microbolometer Thermal Camera, Optical Technologies, Optical Sensors and Measuring Techniques, Nuremberg Exhibition Centre, Germany, 2004.
[21] W. Boyes, Instrumentation Reference Book, Butterworth-Heinemann, 2009.
[22] E.O. Doebelin, A. Cigada, Strumenti e metodi di misura, McGraw-Hill, 2004.
[23] I. Guide, 98-3: 2008/Suppl 1: 2008 Propagation of Distributions Using a Monte Carlo Method, International Organization for Standardization, Geneva, Switzerland, 2008.
[24] F. Angrilli, G. Bianchini, R. Da Forno, S. Debei, G. Fanti, F. Ferri, B. Saggin, Performance verification of a resistance thermometer for atmospheric measurements, in: Proceedings of TEMPMEKO'96, Torino, 10–12 September, 1996.